Supplementary Information

Insight into the Structural and Electronic Nature of Chemically Exfoliated Molybdenum Disulfide Nanosheets in Aqueous Dispersions

Leanddas Nurdiwijayanto,[a,b] Renzhi Ma,[a] Nobuyuki Sakai,[a] and Takayoshi Sasaki[a,b,*]

[a] International Center for Materials Nanoarchitectonics (WPI-MANA), National Institute for Materials Science (NIMS), Namiki 1-1, Tsukuba, Ibaraki 305-0044, Japan.

[b] Graduate School of Pure and Applied Sciences, University of Tsukuba, 1-1-1 Tennodai, Tsukuba, Ibaraki 305-8571, Japan.

* To whom correspondence should be addressed. Email: SASAKI.Takayoshi@nims.go.jp

Contents:

S1. Zeta potential, stability and quality of the nanosheets, and appearance of the dispersions

Chemical exfoliation of MoS_2 nanosheets is initiated by reductive Li intercalation of the MoS_2 host, followed by ultrasonic treatment in water. When the nanosheets are dispersed in a solvent, a specific number of counter-ions is necessary to balance the negative charges of the nanosheets and stabilize the dispersion. In this case, Li ions act as the counter-ions. The amount of Li ions in the stock dispersion after centrifugation cycles were typically 0.2-0.25 per Mo atom, being comparable to the reported values.[1-3] The contents were then adjusted from 0.3 to 10 mole-equivalent units of MoS_2 by adding an appropriate amount of a LiOH solution. Fig. S1 shows zeta potential values of the dispersions as a function of Li contents. The zeta potential values were more negative than −30 mV, indicating good dispersibility due to sufficient mutual repulsion.[4-6]

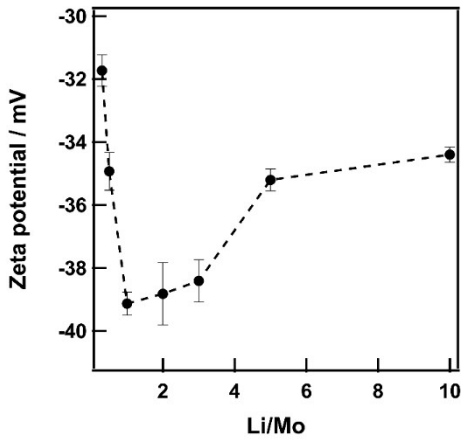

Fig. S1. Zeta potential of MoS_2 nanosheets as a function of Li content in the aqueous dispersion.

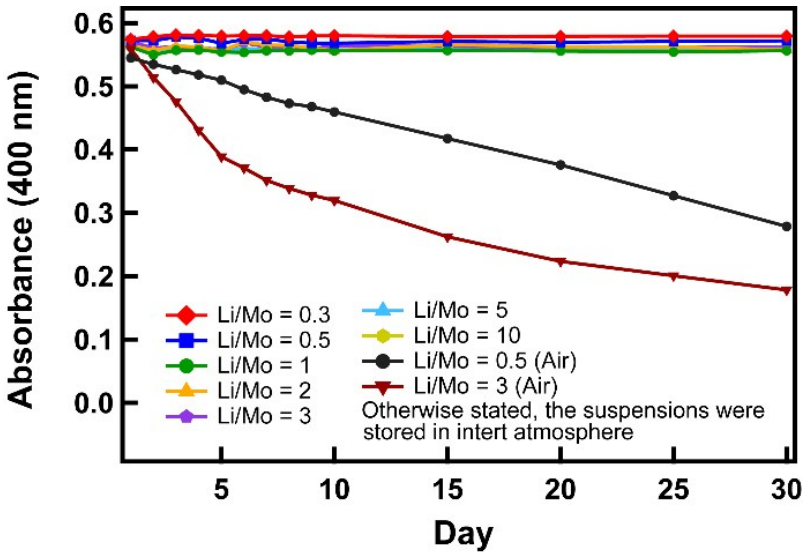

Fig. S2. Change in the absorbance of the dispersion at 400 nm, stored at different atmospheric environments and Li contents.

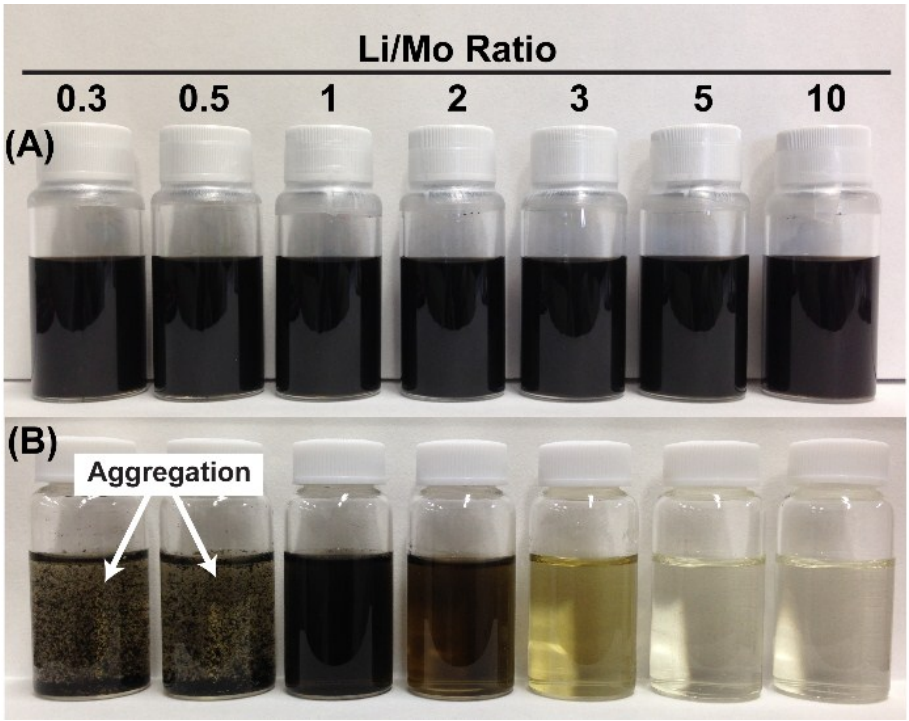

Fig. S3. Photographs of MoS_2 nanosheet dispersions stored for more than 2 months in (A) inert N_2 atmosphere and (B) ambient air. The Li contents were readjusted with the addition of a LiOH solution.

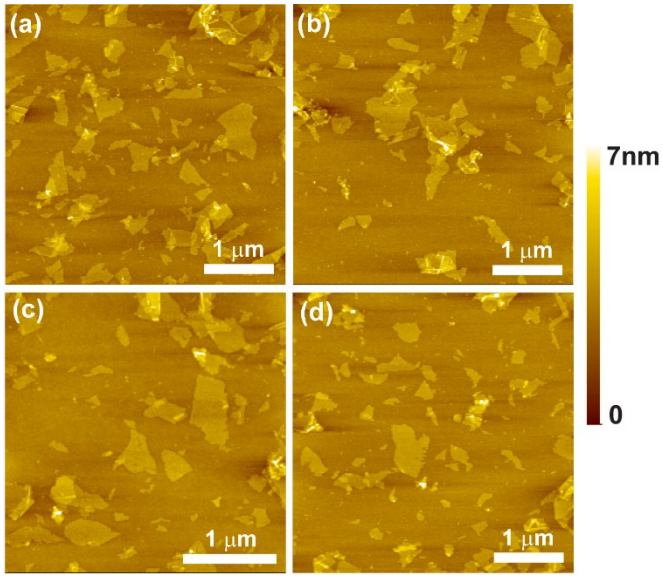

Fig. S4. AFM images of the MoS_2 nanosheets from dispersions stored in inert N_2 atmosphere for 20 days. Li contents were (a) 0.3, (b) 1, (c) 2, and (d) 5 mole equivalent units of the MoS_2.

S2. Additional data for TEM and SAED

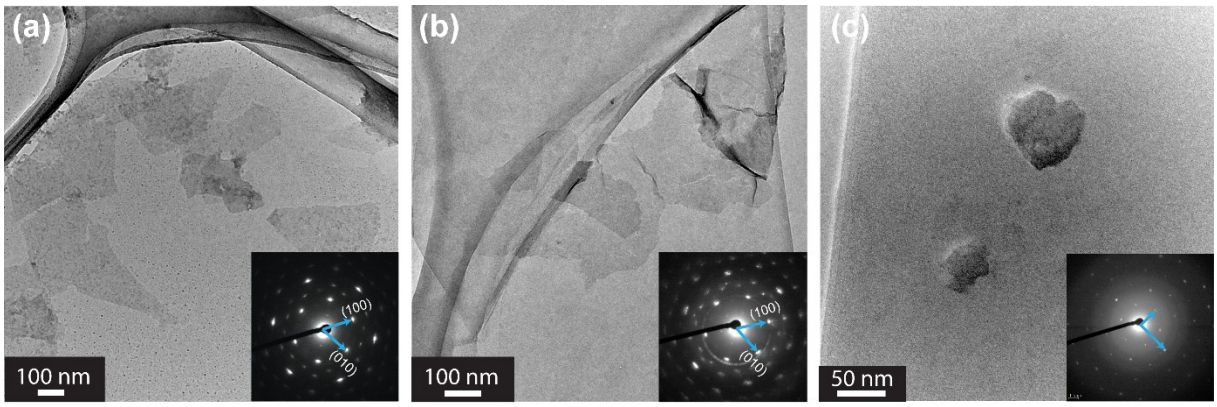

Fig. S5. TEM images of the MoS_2 nanosheets from (a) freshly as-prepared dispersion, and those stored after 1 month in (b) inert N_2 atmosphere and (c) ambient air. Inset: the corresponding electron diffraction patterns.

Electron diffraction patterns of the nanosheets from the freshly-prepared samples and those stored in the inert atmosphere showed six-fold hexagonal spots, with 2-fold periodicity appearing along the (100) and (010) directions (Fig. S5a-b), suggesting the apparent 2×2 superstructure. Note that the lateral dimension of these samples was >500 nm. By contrast, the sample stored in ambient air, which has a substantially small lateral dimension of <50 nm, showed a $\sqrt{3} \times 1$ superstructure. The small sheet may contain only one micro-domain with one sublattice.[7]

S3. Additional data for XPS analysis

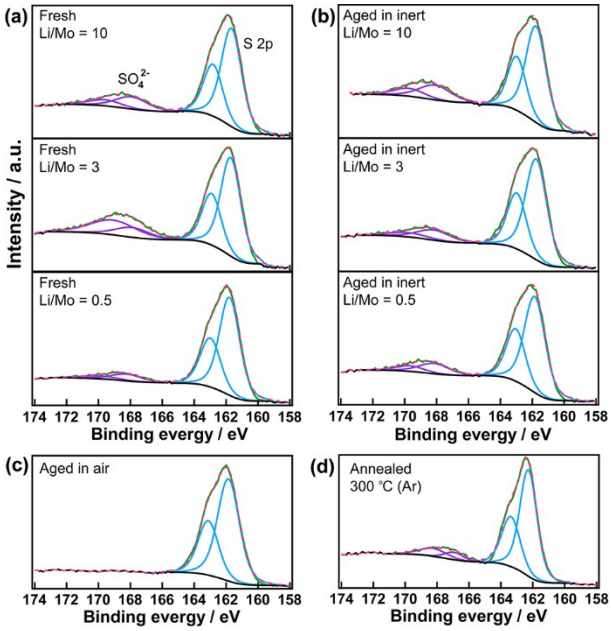

Fig. S6. XPS spectra from the S 2p core levels of the chemically exfoliated MoS_2 nanosheets at various Li contents from (a) freshly as-prepared dispersions, (b) those stored in inert N_2 atmosphere for 2 months, (c) those stored in ambient air for 2 months, and (d) nanosheets annealed at 300 °C in Ar atmosphere.

The S $2p_{3/2}$ and $2p_{1/2}$ binding energies of the MoS_2 nanosheets were identified at approximately 161 to 164 eV, indicating the S^{2-} oxidation state. No significant difference was observed. All the samples, except those exposed to ambient air (Fig. S6c), showed trace amounts of sulfate species (~169 eV). This suggests that the sulfur atoms underwent partial oxidation, which may arise during the specimen preparation of the XPS measurement (the nanosheets were already removed from the dispersions). Note that the preparation and storage of the XPS specimens were carried out in ambient air.

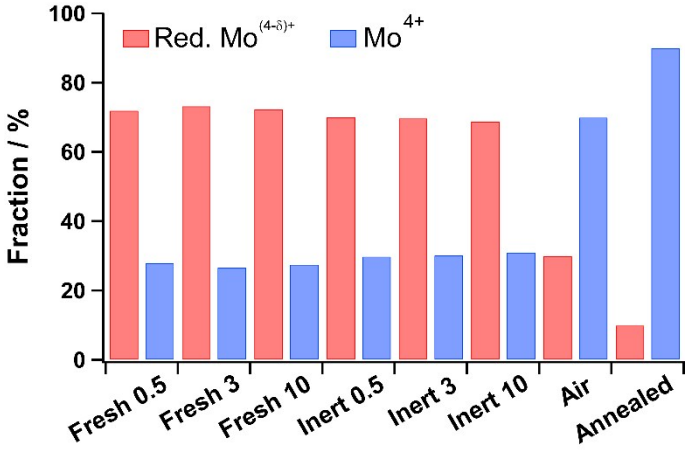

Fig. S7. Fraction of Mo^{4+} and $Mo^{(4-\delta)+}$ oxidation states deduced from XPS analysis of the Mo 3d spectra.

S4. Additional data for 2D structures.

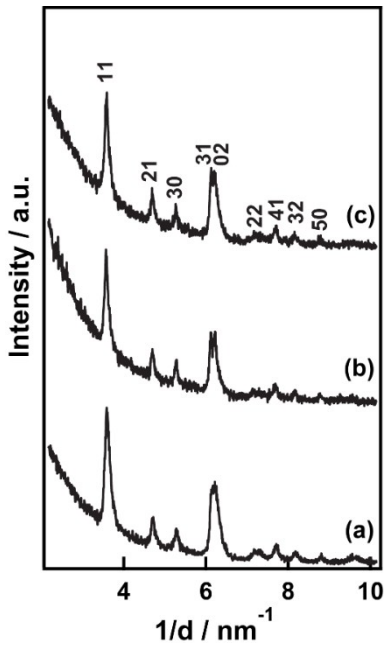

Fig. S8. In-plane XRD patterns of freshly as-prepared MoS_2 nanosheets. Li contents were (a) 0.5, (b) 3, and (c) 10 mole equivalent units of the MoS_2.

Table S1. Summary of 2D lattice symmetry and lattice parameters of chemically exfoliated MoS_2 nanosheets from a variety of treated dispersions. The lattice parameters were refined on the basis of $\sqrt{3} \times 1$ rectangular superstructure.

Sample treatment	Li content (Li/Mo)	2D Symmetry	Lattice parameters		
			a **(nm)**	***b*** **(nm)**	***a/b***
Fresh as-prepared	0.5	Rectangular	0.5679(2)	0.3202(2)	1.7736
	3	Rectangular	0.5695(2)	0.3210(2)	1.7741
	10	Rectangular	0.5687(3)	0.3204(2)	1.7750
Stored in inert N_2	0.5	Rectangular	0.5674(3)	0.3208(2)	1.7687
	3	Rectangular	0.5689(3)	0.3206(3)	1.7745
	10	Rectangular	0.5689(3)	0.3207(3)	1.7739
Exposed to ambient air	0.5	Rectangular	0.5676(2)	0.3194(2)	1.7771
	3	Rectangular	0.5683(3)	0.3191(2)	1.7809
	10	Rectangular	0.5680(4)	0.3193(3)	1.7789

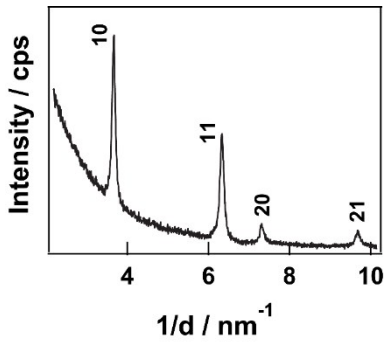

Fig. S9. In-plane XRD pattern of 2H-MoS_2 nanosheets, reverted from the 1T-phase by annealing at 300 °C in Ar atmosphere.

Table S2. Lattice parameters of 2H-MoS_2 refined based on 1×1 hexagonal structure.

Sample Treatment	2D Symmetry	Lattice parameters
		a (nm)
Annealed 300 °C (Ar)	Hexagonal	0.3156(1)

S5. Deconvolution of XRD profile of the restacked nanosheets

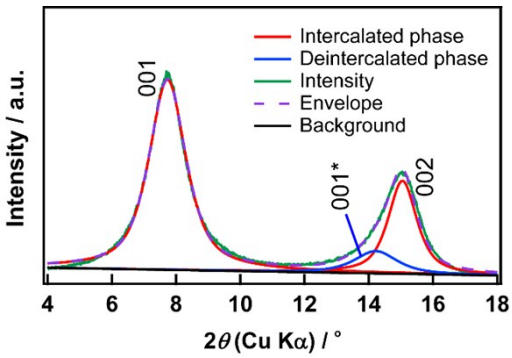

Fig. S10. Deconvolution of the XRD profile of the restacked nanosheets from freshly as-prepared dispersion. The deconvolution was performed on the basis of Pseudo Voigt function by assuming the positions of peaks of the intercalated bilayer-hydrate and deintercalated phases. The area proportion of both phases was deduced from the integrated relative intensities of the 001 peak for the bilayer-hydrate phase and the 001* peak for the deintercalated phase.

Table S3. Area proportion between intercalated bilayer-hydrate and deintercalated phases deduced from deconvolution of the XRD profiles of the restacked nanosheets. Correction of the phase abundance between the two phases is presented.

Dispersion	*d* (nm)			Area proportion		Corrected phase abundance	
aging	001	002	001*	Intercalated	Deintercalated	Intercalated	Deintercalated
Fresh (day 0)	1.144	0.587	0.622	0.90	0.10	0.87	0.13
Aged day 4	1.147	0.590	0.622	0.78	0.22	0.73	0.27
Aged day 7	1.148	0.590	0.622	0.66	0.34	0.60	0.40
Aged day 10	1.160	0.594	0.622	0.51	0.49	0.45	0.55
Aged day 15	1.159	0.590	0.622	0.30	0.70	0.25	0.75

S6. References

1 S. S. Chou, M. De, J. Kim, S. Byun, C. Dykstra, J. Yu, J. Huang and V. P. Dravid, *J. Am. Chem. Soc.*, 2013, **135**, 4584–4587.

2 J. Heising and M. G. Kanatzidis, *J. Am. Chem. Soc.*, 1999, **121**, 11720–11732.

3 A. S. Golub', G. A. Protsenko, L. V. Gumileva, A. G. Buyanovskaya and Y. N. Novikov, *Russ. Chem. Bull.*, 1993, **42**, 632–634.

4 A. Gupta, V. Arunachalam and S. Vasudevan, *J. Phys. Chem. Lett.*, 2015, **6**, 739–744.

5 D. H. Everett, *Basic Principles of Colloid Science*, Royal Society of Chemistry, Cambridge, 1988.

6 S. Gilje, R. B. Kaner, G. G. Wallace, D. A. N. Li, M. B. Mu, M. B. Muller, S. Gilje, R. B. Kaner and G. G. Wallace, *Nat. Nanotechnol.*, 2008, **3**, 101–105.

7 F. Wypych, C. Solenthaler, R. Prins and T. Weber, *J. Solid State Chem.*, 1999, **144**, 430–436.